Clinical Cancer Research

# Inhibition of BUB1 Kinase by BAY 1816032 Sensitizes Tumor Cells toward Taxanes, ATR, and PARP Inhibitors *In Vitro* and *In Vivo*

Gerhard Siemeister, Anne Mengel, Amaury E. Fernández-Montalván, Wilhelm Bone, Jens Schröder, Sabine Zitzmann-Kolbe, Hans Briem, Stefan Prechtl, Simon J. Holton, Ursula Mönning, Oliver von Ahsen, Sandra Johanssen, Arwed Cleve, Vera Pütter, Marion Hitchcock, Franz von Nussbaum, Michael Brands, Karl Ziegelbauer, and Dominik Mumberg

## Abstract

**Purpose:** The catalytic function of BUB1 is required for chromosome arm resolution and positioning of the chromosomal passenger complex for resolution of spindle attachment errors and plays only a minor role in spindle assembly checkpoint activation. Here, we present the identification and preclinical pharmacologic profile of the first BUB1 kinase inhibitor with good bioavailability.

**Experimental Design:** The Bayer compound library was screened for BUB1 kinase inhibitors and medicinal chemistry efforts to improve target affinity and physicochemical and pharmacokinetic parameters resulting in the identification of BAY 1816032 were performed. BAY 1816032 was characterized for kinase selectivity, inhibition of BUB1 signaling, and inhibition of tumor cell proliferation alone and in combination with taxanes, ATR, and PARP inhibitors. Effects on tumor growth *in vivo* were evaluated using human triple-negative breast xenograft models.

**Results:** The highly selective compound BAY 1816032 showed long target residence time and induced chromosome mis-segregation upon combination with low concentrations of paclitaxel. It was synergistic or additive in combination with paclitaxel or docetaxel, as well as with ATR or PARP inhibitors in cellular assays. Tumor xenograft studies demonstrated a strong and statistically significant reduction of tumor size and excellent tolerability upon combination of BAY 1816032 with paclitaxel or olaparib as compared with the respective monotherapies.

**Conclusions:** Our findings suggest clinical proof-of-concept studies evaluating BAY 1816032 in combination with taxanes or PARP inhibitors to enhance their efficacy and potentially overcome resistance.

## Introduction

Cell-cycle deregulation represents one of the classical hallmarks of cancer (1), and consequently cell-cycle arrest is the predominant mode of action of a lot of the cancer drugs on the market including "antimitotics" such as taxanes and vinca alkaloids. In contrast, the concept of cell-cycle checkpoint regulation offers a novel approach to cancer treatment: inactivation of cell-cycle checkpoints is considered to drive tumor cells into cell division despite DNA damage or unattached/misattached chromosomes resulting in a lethal degree of DNA damage or aneuploidy (2).

The spindle assembly checkpoint (SAC, also known as spindle checkpoint or mitotic checkpoint) controls the accurate attachment of microtubules of the spindle device to the kinetochores of the duplicated chromosomes. The SAC is active as long as unattached kinetochores are present and generates a wait signal to give the dividing cell the time to ensure that each kinetochore is attached to a spindle pole, and to correct attachment errors (recently reviewed by Musacchio in ref. 3). The SAC signal is initiated by MPS1-mediated phosphorylation of MELT motifs on the KNL-1 protein to generate docking sites for BUB1/BUB3 dimers, (4) which subsequently recruit BUBR1/BUB3 dimers (5). The inactive open form of MAD2 (o-MAD2) gets converted to the active closed conformation (c-MAD2), which binds CDC20 and BUBR1/BUB3 to form the diffusible mitotic checkpoint complex (MCC), which inhibits the ubiquitin ligase APC/C and thereby delaying anaphase onset. The kinetochore-bound BUB1/BUB3 dimers and the phosphorylation of MAD1/MAD2 complex by MPS1 catalytically accelerate the formation of the MCC; however, the kinase activity of BUB1 has only a modest contribution (6).

BUB1 kinase phosphorylates histone H2A at Thr120 within the centromeric region of the duplicated chromosomes thereby creating binding sites for shugoshin proteins (SGO) 1 and 2, which protect centromeric cohesin from premature degradation (7). Furthermore, phospho-Thr120 histone H2A in conjunction with Haspin-mediated histone H3-Thr3 phosphorylation localizes the chromosome passenger complex (CPC) consisting of INCENP, survivin, borealin, and Aurora kinase B (AURKB) to the centromeres (8). Mouse embryonic fibroblasts (MEF) lacking BUB1

Bayer AG, Muellerstrasse Berlin, Germany.

**Note:** Supplementary data for this article are available at Clinical Cancer Research Online (http://clincancerres.aacrjournals.org/).

Current address for A.E. Fernández-Montalván: Servier Research Institute,125, Chemin de Ronde, 78290 Croissy-sur-Seine, France.

**Corresponding Author:** Gerhard Siemeister, Bayer AG, Muellerstrasse 170–178, Berlin D-13342, Germany. Phone: 4930-4681-2936; Fax: 49 30-4689-2936; E-mail: gerhard.siemeister@bayer.com

**doi:** 10.1158/1078-0432.CCR-18-0628

## Translational Relevance

Microtubule-targeting agents are a cornerstone in the treatment of patients suffering from breast, ovarian, prostate, and other cancers. However, recurrence of treatment-refractory tumors still represents a challenge. Interference with cell-cycle checkpoints opens the opportunity to drive tumor cells into abortive cell division in the presence of DNA damage or misattached chromosomes. We describe the preclinical profile of BAY 1816032, a novel, bioavailable inhibitor of the catalytic activity of the mitotic checkpoint protein BUB1, which is involved in centromere cohesion and attachment error correction. Inhibition of BUB1 sensitizes tumor cells toward paclitaxel and docetaxel, and toward ATR inhibitors and PARP inhibitors. In xenograft models of triple-negative breast cancer BAY 1816032 in combination with paclitaxel or olaparib strongly delayed outgrowth of tumors under treatment as compared with paclitaxel or olaparib single agents. This study supports the clinical evaluation of the BUB1 kinase inhibitor in combination with taxanes or PARP inhibitors.

catalytic activity failed to concentrate AURKB at the inner centromeres, showed reduced phosphorylation of centromeric substrates of AURKB, and were compromised in their ability to efficiently correct spindle attachment errors (9). Specific inhibition of BUB1 kinase activity by low molecular weight inhibitors caused persistent sister chromatid cohesion, reduced levels of SGO1 and SGO2 at mitotic centromeres, and redistributed SGO2 to chromosome arms (10). Furthermore, CPC subunits were partially displaced from centromeres with a local reduction of AURKB activity, reduced association of the AURKB effector protein mitotic centromere–associated kinesin (MCAK, Kif2C), and a redistribution of AURKB over the chromosome arms. Localization of AURKB activity and of the microtubule-depolymerizing kinesin MCAK at the centromeric region is essential for the resolution of microtubule–kinetochore attachment errors such as syntelic and merotelic attachments (11). Dyslocalization of AURKB due to BUB1 kinase inactivation strongly compromises the cells' ability to resolve attachment errors and results in an increased rate of chromosome alignment defects, in particular, in presence of attachment error–inducing agents such as microtubule stabilizer paclitaxel (10).

The previously published highly selective BUB1 kinase inhibitors, BAY-320 and BAY-524, represent excellent tools to dissect the role of BUB1 catalytic activity in biochemical and cellular experimental settings (6, 10); however, due to their limited pharmacokinetic properties they are not suitable for *in vivo* investigations. Here, we present for the first time the identification and the preclinical profile of the novel BUB1 kinase inhibitor BAY 1816032. In particular, we demonstrate additive and more than additive efficacy upon combination of BUB1 kinase inhibition with taxanes, as well as with PARP inhibitors in cellular and in tumor xenograft models.

## Materials and Methods

### Chemicals and antibodies

BAY 1816032 and olaparib were synthesized at Bayer AG. Docetaxel was purchased from Sanofi-Aventis Deutschland GmbH, paclitaxel from Sigma-Aldrich or from Lapharm GmbH (for *in vivo* studies), cisplatin from Sigma-Aldrich. Anti–phospho-SMAD2 (Ser465/467), anti–phospho-SMAD3 (Ser423/425), anti-SMAD2, and anti-SMAD3 antibodies were from Cell Signaling Technology and anti-GAPDH antibody from Zytomed.

### BUB1 protein

Two different cDNAs encoding BUB1 (704-1085) for ITC and BUB1 (730-1085) for X-ray were integrated into a gateway-compatible pVL 1393 vector. The resulting plasmids encode for a N-terminal His-Tag followed by a Thrombin cleavage site and the BUB1 cDNA. High titer recombinant baculoviruses were obtained with the Flashbac system according to the manufacturer's protocol (Oxford Expression Technologies). For large-scale production of recombinant protein, Trichoplusia ni cells, at the density of $2 \times 10^6$ cells/mL, were infected with high titer viral stock at a multiplicity of infection (MOI) of one. Cells were harvested 48 hours postinfection, flash frozen in liquid nitrogen, and stored at −80°C. BUB1 protein was purified from cell lysates by HisTrap column (GE Healthcare) chromatography, followed by thrombin cleavage and size exclusion chromatography (Superdex 200, GE Healthcare). Purified protein was flash frozen in liquid nitrogen and stored at −80°C.

### Kinase assay and selectivity profiling

Inhibitory activities BAY 1816032 toward BUB1 were quantified using a time-resolved fluorescence energy transfer (TR-FRET) kinase assay and the recombinant catalytic domain of human BUB1 (amino acids 704–1085) as previously published (12). Mode of action and $K_i$ determination were performed with the same assay, following general procedures described in ref. 13, and explained in detail in the Supplementary Information. Kinase selectivity was initially determined at 100 and 1,000 nmol/L, in an active site-directed competition-binding assay measuring 403 human kinases (Lead Hunter, DiscoverX Kinome Scan) followed by $K_d$ determination for those kinases inhibited by >60% at 100 nmol/L.

### Binding kinetics

Target-binding kinetics of the BUB1 inhibitors shown in this article were determined in solution with the kinetic probe competition assay (kPCA) described in ref. 14, using Kinase Tracer 236 from Invitrogen (Life Technologies) as fluorescent probe. Solid-phase–binding kinetics measurements were performed with a surface plasmon resonance (SPR) assay, following standard protocols from Biacore (GE Healthcare). Avi-Tag biotinylated BUB1 catalytic domain was used in both methods. Furthermore, details on experimental procedures are described in the Supplementary information.

### Crystallography

BUB1 kinase domain crystals were grown at 4°C using the sitting-drop method by mixing 1 μL of protein/BAY 1816032 (14.7 mg/mL) with 1 μL of well solution (100 mmol/L Tris-HCl pH 7.26, 200 mmol/L $MgCl_2$, 20% PEG 3350, 5% gylcerol). A single crystal was briefly immersed in cryo-protection solution consisting of mother liquor supplemented with 10 mmol/L compound and 20% glycerol and then flash frozen in liquid nitrogen. X-ray data were collected on the Helmholtz-Zentrum Berlin beamline 14-1 at a wavelength of 0.91814 Å using a PILATUS detector. Data were integrated, scaled, and merged using

the programs XDS and AIMLESS (15, 16). The structure was solved by molecular replacement using the program Phaser (17). Initial electron density maps clearly indicated binding of the compound. The model was refined through iterative manual and maximum-likelihood refined using the programs COOT and REFMAC5 (15, 18). Statistics for the final model are given in the Supplementary Table S6. Coordinates and structure factors have been submitted to the PDB database and are accessible with the code 6F7B.

### Cell lines and cell culture

Tumor cell lines were obtained either from the ATCC or from the German Collection of Microorganisms and Cell Cultures; SUM-149 cells were from Asterand Bioscience, and HeLa-MaTu-ADR cells were from Epo GmbH. Authentication of all human cell lines used was performed at the German Collection of Microorganisms and Cell Cultures via PCR-based DNA profiling of polymorphic short tandem repeats (for cell line details see Supplementary Table S2). Cells were propagated under the suggested growth conditions in a humidified 37°C incubator.

### *In vitro* combination assay, phospho-histone assay, and live-cell imaging

*In vitro* combination assays have been performed as described before (10) and detailed in the Supplementary information. Inhibition of histone H2A-Thr120 phosphorylation and of histone H3-Ser10 phosphorylation was determined as described previously (10, 19).

For fluorescence time-lapse imaging, cells were imaged using a Perkin Elmer OPERA microscope equipped with a climate-controlled environment chamber. HeLa (ATCC CCL-2) cells stably expressing H2B-GFP were plated with a density of 3,000 cells per well in a 384-well microtiter plate in 20 μL cell culture medium, and preincubated overnight at 37°C. The cells were treated with the substances in the indicated concentrations in triplicates. Images were taken immediately after the substances were added. Image acquisition was repeated every 6 minutes for 24 hours. Image evaluation was performed using Molecular Device's MetaXpress software, which arranged individual images in time-dependent image stacks.

### Pharmacokinetic investigations

Pharmacokinetic studies were performed in male Wistar rats, female CD1 mice, and female Beagle dog. BAY 1816032 was solubilized in 50% polyethylene glycol 400, 40% water, and 10% ethanol for intravenous and oral dosing in rats, mice, and dog. In pharmacokinetic studies, plasma samples were collected after 2 minutes, 5 minutes, 15 minutes, 30 minutes, 45 minutes, 1 hour, 2 hours, 4 hours, 6 hours, 8 hours, 24 hours after intravenous administration and after 8 minutes, 15 minutes, 30 minutes, 45 minutes, 1 hour, 2 hours, 4 hours, 6 hours, 8 hours, 24 hours after oral administration and precipitated with ice-cold acetonitrile (1:5). Supernatants were analyzed via LC/MS-MS. Pharmacokinetic parameters were estimated from the plasma concentration data, for example, using the lin-log trapezoidal rule for AUC estimation. Maximal plasma concentrations ($C_{max}$) and time thereof ($T_{max}$) were taken directly from the concentration–time profiles.

### Animal efficacy studies

Housing and handling of animals was in strict compliance with European and German Guidelines for Laboratory Animal Welfare. SUM-149 xenografts were inoculated into the inguinal region of female athymic NMRI *nu/nu* mice (Taconic); MDA-MB-436 xenografts were inoculated into the fourth mammary fad pad of female NOD-SCID mice (NOD.CB17-Prkdc$^{scid}$/J, Charles River, Iffa Credo). When tumors reached a size of approximately 20 to 40 mm$^2$, depending on growth of the tumor model, animals were randomized to treatment and control groups (12 mice/group) and treated orally with vehicle (90% polyethylene glycol 400, 10% Ethanol), BAY 1816032, and/or paclitaxel, docetaxel, or olaparib [dissolved in 10% DMSO, 90% (10% HPbetaCD in PBS, pH 7.8)] as indicated in tables and figure legends (for details, see Supplementary Methods).

## Results

### Identification of BAY 1816032: a highly selective BUB1 kinase inhibitor

A high-throughput screening (HTS) of the Bayer compound collection (2.4 million entities, $n = 1$) was performed using the BUB1 kinase activity assay with TR-FRET readout described in ref. 20. The quality of the HTS was excellent, with the majority of the plates tested showing a $Z'$-factor >0.5, a parameter which reveals good separation of vehicle (neutral) and inhibition controls. The compound activities followed a normal distribution, which allowed setting a 3δ of the neutral controls as threshold for hit selection (Supplementary Fig. S1A). The resulting hits were retested at $n = 4$ (Supplementary Fig. S1B, top) and those for which inhibition was confirmed were further analyzed in dose response (Supplementary Fig. S1B, bottom). $IC_{50}$ hits were prioritized according to their "on-target" activity, novelty, and selectivity. Among them a "single" hit (Fig. 1A, left) arose from a relative large sublibrary of related indazoles with submicromolar activity and ATP-competitive behavior (Supplementary Fig. S1C). The specific binding of this compound was confirmed with a kinetic probe competition assay (kPCA) and SPR (Supplementary Fig. S1D), as well as with isothermal titration calorimetry (ITC; Table 1). Furthermore, an X-ray structure of this compound in complex with the BUB1 kinase domain revealed the molecular mode of action (data not shown). This binding mode is highly conserved with that of the optimized BAY 1816032 compound (Fig. 1G).

Medicinal chemistry efforts resulted in the identification of the lead compound (Fig. 1A, center), which showed a 10-fold improvement in affinity (Table 1). Interestingly, the ATP-competitive behavior of this compound was overturned by a 30-minute preincubation with BUB1. This result pointed to a prolonged residence time of the inhibitor, an assumption, which was readily confirmed by analysis of the binding to BUB1 with kPCA and SPR (Table 1). The lead compound showed cellular activity in mechanistic and functional assays (Table 1). Furthermore, structural variations to improve the physicochemical and pharmacokinetic properties led to the identification of BAY 1816032 featuring high potency, long target residence time, and good oral bioavailablity. The structure–activity and absorption, distribution, metabolism, and excretion property optimization leading to BAY 1816032 will be the subject of a future publication.

BAY 1816032 (Fig. 1A, right) inhibits the recombinant catalytic domain of human BUB1 with an $IC_{50}$ of 6.1 ± 2.5 nmol/L in presence of 10 μmol/L ATP. In an equilibrium-binding assay BAY 1816032 competed with a fluorescein-labeled BUB1-specific probe with an $IC_{50}$ of 1.0 ± 0.5 nmol/L ($K_i = 0.5 \pm 0.3$ nmol/L), and in the KINOMEscan panel it was tested with a

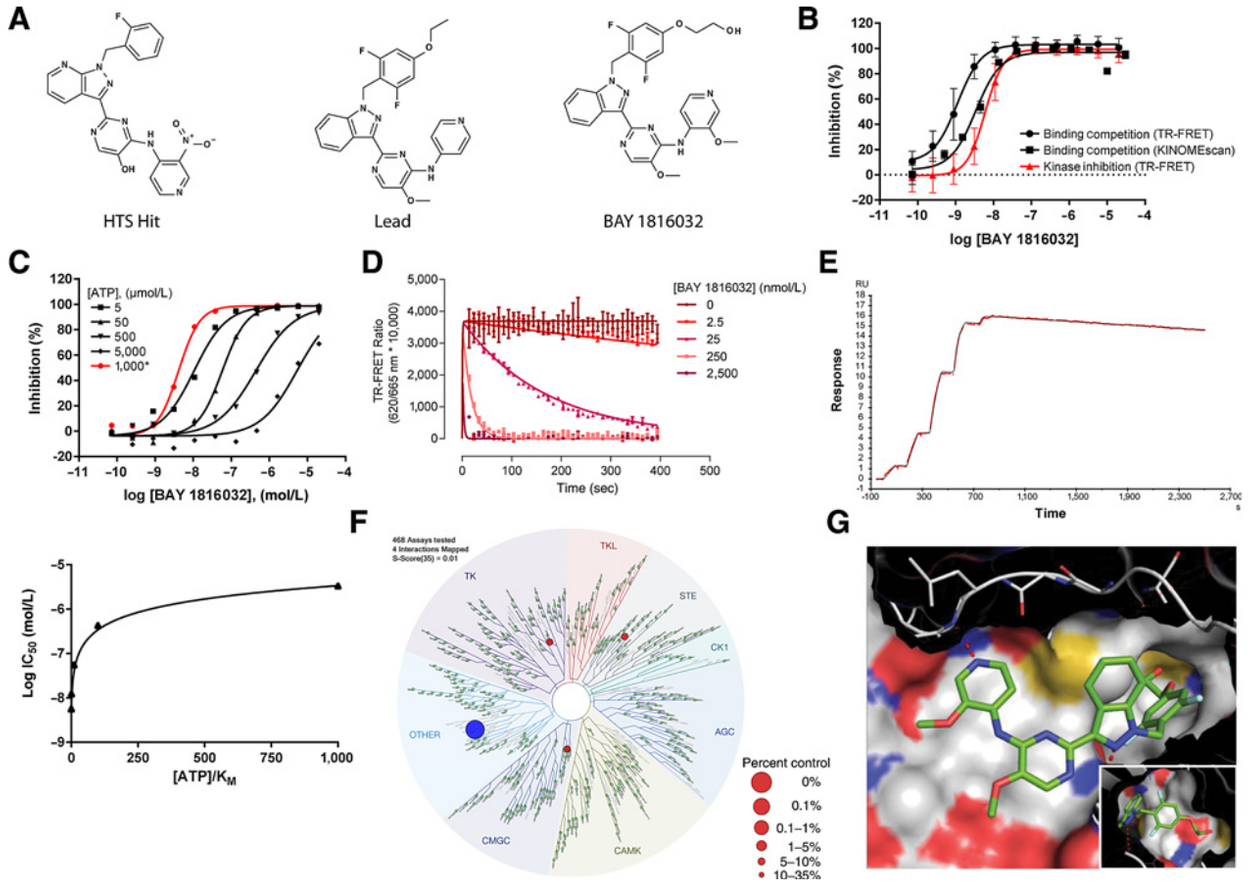


**Figure 1.**

Identification and characterization of BAY 1816032. **A,** Chemical structures of the compounds described in this publication. **B,** Activities of BAY 1816032 in orthogonal biochemical activity and binding assays. Potency values derived from these experiments are shown in Table 1. **C,** Biochemical mode of action study of BAY 1816032 using the biochemical TR-FRET assay. The top panel shows dose–response inhibition curves (in black) obtained at the ATP concentrations as indicated without prior preincubation of the compound with BUB1. The red curve was also measured with 1 mmol/L ATP but the compound and BUB1 were preincubated for 15 minutes before start of the enzymatic reaction. The bottom panel shows the fit of the $IC_{50}$ values obtained at different ATP concentrations (without preincubation) to the Cheng–Prussof equation (39), resulting in the $K_i$ value shown in Table 1. **D,** kPCA traces corresponding to the displacement of Invitrogen's Kinase Tracer 236 by increasing concentrations of BAY 1816032. Fitting of these curves to the Motulsky and Mahan competitive kinetics model (40) resulted in the affinity and rate constants shown in Table 1. **E,** SPR single-cycle kinetics sensorgram corresponding to the titration of BAY 1816032 as indicated in the Methods section. Fitting this sensorgram to the Langmuir model yielded the affinity and rate constants shown in Table 1. **F,** Selectivity profile of BAY 1816032 probed at a concentration of 1,000 nmol/L against 403 human kinases of the DiscoveRx KINOMEscan panel. Spot size corresponds to the remaining activity of the tested kinases as indicated in the legend. The image was generated using TREEspot Software Tool and reprinted with permission from KINOMEscan, a division of DiscoveRx Corporation, © DISCOVERX CORPORATION 2010. **G,** Crystal structure of the BUB1 kinase domain in complex with BAY 1816032 (C, N, O, and F atoms are colored green, blue, red, and cyan, respectively).

$K_d$ of 3.3 nmol/L (Fig. 1B). As shown for the hit and lead compounds, it is an ATP-competitive inhibitor with a $K_i$ of $1.2 \pm 0.7$ μmol/L. In contrast to the HTS hit and similarly to the lead compound, the shift in $IC_{50}$ resulting from an increase in the ATP concentrations is reversed by preincubation of the compound with the BUB1 catalytic domain (Fig. 1C). Here again, BAY 1816062 showed slow binding kinetics in kPCA with rate constants for the association (kon) and dissociation (koff) of $4.1 \pm 0.5 \times 10^5$ L·mol$^{-1}$s$^{-1}$ and $2.2 \pm 1.0 \times 10^{-4}$ s$^{-1}$, respectively, and an affinity constant ($K_d$) of $1.2 \pm 0.9$ nmol/L (Fig. 1D; Table 1). These values were confirmed in SPR experiments (Fig. 1E; Table 1), and the residence times calculated from kPCA and SPR ($t_{1/2}$ of 87 minutes and 203 minutes, respectively) are expected to give full target coverage during the time required for a standard mitosis. Quantitative measurements of BAY 1816032 interactions with 403 human kinases, using active site-directed competition-binding assays, revealed that besides BUB1 only three additional kinases (LOK/STK10, DMPK2, and DDR1) were hit at a compound concentration of 100 nmol/L (Fig. 1F). The respective $K_d$s of 57, 850, and 2,300 nmol/L for these kinase contrasted with the $K_d$ of 3.3 nmol/L mentioned above, demonstrating at least 17-fold binding selectivity of BAY 1816032 for BUB1 over the most prominent off-target kinases (Supplementary Table S1). For DYRK1B and GSK3A found in the initial screen, binding of BAY 1816032 was not reproduced upon $K_d$ determination.

To better understand the BAY 1816032 inhibition mechanism, we determined an X-ray structure in complex with the BUB1

**Table 1.** Binding parameters of BAY 1816032 and related compounds discussed in this paper

| | | Compound | | |
|---|---|---|---|---|
| **Binding parameter** | **Method** | **HTS Hit** | **Lead** | **BAY 1816032** |
| $IC_{50}$ (mol/L) | Kinase activity (10 μmol/L ATP) | 5.0E−8 ± 1.1E−8 | 6.7E−9 ± 4.52E−9 | 6.1E−9 ± 2.4E−9 |
| $IC_{50}$ (mol/L) | Kinase activity (1 mmol/L ATP) | 5.2E−6 ± 8.8E−7 | 7.3E−9 ± 4.7E−9 | 4.3E−9 ± 4.5E−10 |
| $K_i$ (mol/L) | Kinase activity | 2.0E−7 ± 4.7E−9 | 1.0E−9 ± 2.7E−11 | 3.4E−9 ± 3.8E−10 |
| $IC_{50}$ (mol/L) | Binding competition (ePCA) | 2.6E−8 ± 2.6E−9 | 3.4E−9 ± 3.2E−9 | 1.0E−9 ± 4.8E−10 |
| $K_d$ (mol/L) | Binding competition (KINOMEscan) | n.d. | n.d. | 3.3E−9 |
| $K_d$ (mol/L) | Binding competition (kPCA) | 9.5E−8 ± 7.3E−9 | 3.8E−9 ± 6.4E−9 | 1.3E−9 ± 9.4E−10 |
| $k_{on}$ ($L \cdot mol^{-1} \cdot s^{-1}$) | Binding competition (kPCA) | 1.2E5 ± 2.5E2 | 3.8E5 ± 4.4E5 | 4.1E5 ± 5.1E4 |
| $k_{off}$ ($s^{-1}$) | Binding competition (kPCA) | 1.5E−3 ± 4.1E−5 | 2.4E−4 ± 2.2E−4 | 2.2E−4 ± 1.0E−4 |
| $K_d$ (mol/L) | Binding (SPR) | 3.0E−8 | 1.7E−9 | 2.1E−9 |
| $k_{on}$ ($L \cdot mol^{-1} \cdot s^{-1}$) | Binding (SPR) | 1.2E6 | 2.6E5 | 2.5E4 |
| $k_{off}$ ($s^{-1}$) | Binding (SPR) | 0.04 | 2.6E−4 | 5.1E−5 |
| $K_d$ (mol/L) | Binding (ITC) | 5.2E−8 ± 1.2E−8 | 3.4E−8 ± 3.4E−8 | n.d. |
| ΔH ($cal \cdot mol^{-1}$) | Binding (ITC) | −16955 ± 145 | −19627 ± 228 | n.d. |
| ΔG ($cal \cdot mol^{-1}$) | Binding (ITC) | −9964 ± 130 | −10668 ± 682 | n.d. |
| TΔS ($cal \cdot mol^{-1}$) | Binding (ITC) | 6991 ± 15 | 8934 ± 916 | n.d. |

NOTE: Values represent the mean of at least two independent experiments with two technical replicates. In cases where SDs are not indicated, a single experiment with three or more replicates was conducted. Experimental details to the methods used are given in the Materials and Methods section.

kinase domain (Fig. 1G). Consistent with the enzymatic data, the compound was shown to bind in the ATP-binding pocket. A single hydrogen bond is formed between the pyridine nitrogen and the backbone Tyr869 nitrogen that is located in the kinase hinge region. The excellent compound selectivity results from the benzyl–pyrazole ring that inserts into the BUB1 kinase–unique space created by the small Gly866 gatekeeper residue. Adjacent to the gatekeeper residue, the substituted benzyl ring inserts into a flexible secondary-binding pocket within the kinase active site that is formed by induced fit upon compound binding.

### Characterization of cellular activity

BAY 1816032 abrogated histone H2A-Thr120 phosphorylation, the best validated substrate of BUB1 kinase, in nocodazole-arrested HeLa cells after 1 hour of compound incubation with an $IC_{50}$ of 29 ± 23 nmol/L demonstrating its potent intracellular inhibition of BUB1 kinase activity. However, in line with previous findings (10), the functionality of the spindle assembly checkpoint was not affected by BUB1 kinase inhibition as indicated by persistent histone H3-Ser10 phosphorylation in nocodazole-arrested HeLa cells upon 4-hour incubation at concentrations up to 10 μmol/L, which is in contrast to MPS1 inhibitors BAY 1161909 and BAY 1217389, which had been reported to override the SAC with $IC_{50}$ values of 56 nmol/L and 0.11 nmol/L, respectively (19).

Antiproliferative activity as single agent was investigated on a panel of 43 human and mouse tumor cell lines from various indications (Supplementary Table S2). BAY 1816062 inhibited tumor cell proliferation with a median $IC_{50}$ of 1.4 μmol/L in a very uniform manner (range of measured $IC_{50}$'s between 0.5 and 5.8 μmol/L). No highly sensitive or highly insensitive cell line was found within this panel, which precluded approaches to identify biomarkers for cellular sensitivity.

LOK, the most prominent off-target kinase of BAY 1816032 found in biochemical binding assays, phosphorylates ezrin-Thr567 (21). In contrast to erlotinib, which inhibits LOK, BAY 1816032 did not inhibit ezrin/radixin/moesin phosphorylation in Jeg-3 and HCT116 cells (Supplementary Fig. S2A) corroborating the exquisite selectivity of BAY 1816032. On the basis of BUB1 siRNA knockdown and BUB1 inhibition using the bulky ATP analog 2OH-BNPP1 (22) SMAD2/3 proteins were recently proposed as substrates of BUB1 kinase upon TGFβ stimulation of A549 cells (23). 2OH-BNPP1 represents a rather unselective kinase inhibitor with activity at least against the tyrosine kinases PDGF-Rβ, CSF1-R, VEGF-R2, VEGF-R3, in addition to BUB1 and with $IC_{50}$s in the range of 30 to 100 nmol/L (Supplementary Table S3). In contrast to SB-431542, an inhibitor of TGFβ type I receptors (24), and to 2OH-BNPP1, the highly selective BUB1 inhibitors BAY 1816032, as well as BAY-320 (10) did not block TGFβ-stimulated SMAD2/3 phosphorylation in A549 cells even at concentrations up to 30 μmol/L (Supplementary Fig. S2B) suggesting that BUB1 kinase activity is not essential for TGFβ signaling toward SMAD2/3 and that other kinases inhibited by 2OH-BNPP1 may be involved.

### BAY 1816032 sensitizes tumor cells toward taxanes, ATR inhibitors, and PARP inhibitors

Dose–response combination studies demonstrated synergistic or at least additive antiproliferative effects of BAY 1816032 when combined with either paclitaxel or docetaxel in HeLa, as well as in triple-negative breast cancer, non–small cell lung, glioblastoma, and prostate cancer cells (Table 2). The combination with cisplatin was antagonistic, which is in line with the mode of action of cisplatin-forming DNA adducts and cross-links leading to cell-cycle arrest in S- or $G_2$-phase of the cell cycle. This finding was further corroborated by the predominantly antagonistic effects of irinotecan (SN-38), 5-fluorouracil, and gemcitabine upon combination with BAY 1816032 (Supplementary Table S4). Yang and colleagues (25) reported that phosphorylation of BUB1 by ATM kinase is required for optimal DNA damage response upon exposure to ionizing radiation. As ATM loss-of-function mutations are synthetically lethal with interference with ATR signaling (26), we hypothesized that inhibition of BUB1 kinase could be synthetically lethal with ATR kinase inhibition as well. Indeed, the combination of the ATR inhibitor AZ20 (27) with BAY 1816032 showed synergy in the ATM-proficient MDA-MB-468 cells, whereas a slight antagonism was observed with ATM-deficient or low ATM protein–expressing HT-144 and GRANTA-519 cells (Table 2). Supportive data were generated from combinations of BAY 1816032 with the ATR inhibitors AZD6739 (28), VX-970 (29), or BAY 1895344 (30), and the ATM inhibitor KU 60019 demonstrating synergy between BAY 1816032 and ATR inhibition in

**Table 2.** *In vitro* combination of BAY 1816032 with paclitaxel, docetaxel, cisplatin, AZ20, and olaparib

| Cell line | Single-agent $IC_{50}$ | Single-agent concentrations used in combination and combination index $CI_{50}$ | | | | | | | | | Single agent $IC_{50}$ |
|---|---|---|---|---|---|---|---|---|---|---|---|
| | **BAY 1816032** | **BAY 1816032 plus paclitaxel** | | | | | | | | | **Paclitaxel** |
| HeLa | 1.9E−06 | 7.6E−07 | 5.3E−07 | 3.8E−07 | 2.8E−07 | 2.1E−07 | 1.6E−07 | 1.3E−07 | 8.4E−08 | 4.8E−08 | |
| | | 8.4E−10 | 1.3E−09 | 1.6E−09 | 1.8E−09 | 2.1E−09 | 2.4E−09 | 2.9E−09 | 3.4E−09 | 4.3E−09 | 6.6E−09 |
| | | **0.53** | **0.48** | **0.44** | **0.42** | **0.43** | **0.45** | **0.51** | **0.55** | **0.68** | |
| SUM-149 | 1.9E−06 | 1.4E−06 | 9.0E−07 | 6.2E−07 | 4.7E−07 | 3.7E−07 | 2.4E−07 | 1.7E−07 | 1.0E−07 | 4.4E−08 | |
| | | 4.6E−10 | 6.7E−10 | 8.0E−10 | 9.4E−10 | 1.1E−09 | 1.1E−09 | 1.2E−09 | 1.2E−09 | 1.2E−09 | 1.3E−09 |
| | | **1.09** | **1.01** | **0.96** | **0.99** | **1.06** | **0.96** | **1.01** | **1.02** | **0.96** | |
| MDA-MB-436 | 1.8E−06 | 1.1E−06 | 7.9E−07 | 4.9E−07 | 4.1E−07 | 3.1E−07 | 2.0E−07 | 1.5E−07 | 1.0E−07 | 4.8E−08 | |
| | | 1.2E−09 | 2.0E−09 | 2.1E−09 | 2.8E−09 | 3.1E−09 | 3.1E−09 | 3.5E−09 | 4.1E−09 | 4.3E−09 | 4.9E−09 |
| | | **0.87** | **0.85** | **0.7** | **0.79** | **0.79** | **0.74** | **0.8** | **0.89** | **0.90** | |
| NCI-H1299 | 1.8E−06 | 1.3E−06 | 8.6E−07 | 6.8E−07 | 5.5E−07 | 4.1E−07 | 3.3E−07 | 2.6E−07 | 1.7E−07 | 1.0E−07 | |
| | | 4.2E−10 | 6.5E−10 | 8.8E−10 | 1.1E−09 | 1.2E−09 | 1.5E−09 | 1.8E−09 | 2.0E−09 | 2.7E−09 | 5.8E−09 |
| | | **0.76** | **0.58** | **0.52** | **0.49** | **0.44** | **0.43** | **0.45** | **0.44** | **0.53** | |
| 22RV1 | 7.9E−07 | 6.0E−07 | 3.6E−07 | 2.4E−07 | 2.0E−07 | 1.3E−07 | 1.0E−07 | 6.6E−08 | 4.8E−08 | 2.2E−08 | |
| | | 2.0E−09 | 2.7E−09 | 3.1E−09 | 4.0E−09 | 3.8E−09 | 4.7E−09 | 4.6E−09 | 5.8E−09 | 5.9E−09 | 6.3E−09 |
| | | **1.08** | **0.89** | **0.79** | **0.89** | **0.75** | **0.88** | **0.81** | **0.98** | **0.96** | |
| H4 | 1.4E−06 | 5.7E−07 | 3.8E−07 | 2.6E−07 | 2.1E−07 | 1.6E−07 | 1.4E−07 | 1.1E−07 | 8.0E−08 | 5.3E−08 | |
| | | 6.3E−10 | 9.5E−10 | 1.1E−09 | 1.4E−09 | 1.6E−09 | 2.1E−09 | 2.5E−09 | 3.2E−09 | 4.7E−09 | 1.1E−08 |
| | | **0.46** | **0.36** | **0.29** | **0.29** | **0.27** | **0.30** | **0.31** | **0.36** | **0.49** | |
| | **BAY 1816032** | **BAY 1816032 plus docetaxel** | | | | | | | | | **Docetaxel** |
| NCI-H1299 | 3.0E−06 | 1.4E−06 | 8.3E−07 | 5.8E−07 | 4.4E−07 | 3.0E−07 | 2.3E−07 | 1.7E−07 | 1.1E−07 | 6.3E−08 | |
| | | 4.5E−10 | 6.2E−10 | 7.4E−10 | 8.9E−10 | 8.9E−10 | 1.1E−09 | 1.2E−09 | 1.4E−09 | 1.7E−09 | 2.4E−09 |
| | | **0.65** | **0.54** | **0.50** | **0.52** | **0.47** | **0.52** | **0.54** | **0.60** | **0.74** | |
| 22RV1 | 6.5E−07 | 5.1E−07 | 3.1E−07 | 2.1E−07 | 1.5E−07 | 1.1E−07 | 8.0E−08 | 6.4E−08 | 3.9E−08 | 1.9E−08 | |
| | | 1.7E−10 | 2.3E−10 | 2.7E−10 | 3.0E−10 | 3.4E−10 | 3.6E−10 | 4.5E−10 | 4.6E−10 | 5.2E−10 | 5.7E−10 |
| | | **1.09** | **0.87** | **0.80** | **0.75** | **0.76** | **0.75** | **0.88** | **0.87** | **0.93** | |
| H4 | 1.2E−06 | 5.1E−07 | 3.2E−07 | 2.3E−07 | 1.7E−07 | 1.4E−07 | 1.1E−07 | 8.9E−08 | 6.7E−08 | 3.9E−08 | |
| | | 1.7E−10 | 2.4E−10 | 3.0E−10 | 3.4E−10 | 4.2E−10 | 5.0E−10 | 6.2E−10 | 8.1E−10 | 1.1E−09 | 1.8E−09 |
| | | **0.51** | **0.40** | **0.35** | **0.33** | **0.35** | **0.37** | **0.42** | **0.51** | **0.62** | |
| | **BAY 1816032** | **BAY 1816032 plus cisplatin** | | | | | | | | | **Cisplatin** |
| HeLa | 1.8E−06 | 1.8E−06 | 1.7E−06 | 1.8E−06 | 1.5E−06 | 1.4E−06 | 1.1E−06 | 8.7E−07 | 6.5E−07 | 1.9E−07 | |
| | | 6.5E−07 | 1.4E−06 | 2.6E−06 | 3:3E−06 | 4.7E−06 | 5.6E−06 | 6.8E−06 | 8.6E−06 | 5.6E−06 | 4.8E−06 |
| | | **1.14** | **1.28** | **1.57** | **1.53** | **1.79** | **1.82** | **1.92** | **2.18** | **1.29** | |
| NCI-H460 | 3.2E−06 | 3.7E−06 | 3.6E−06 | 3.2E−06 | 2.8E−06 | 2.7E−06 | 2.6E−06 | 3.0E−06 | 2.4E−06 | 1.5E−06 | |
| | | 1.2E−07 | 2.7E−07 | 4.2E−07 | 5.6E−07 | 8.0E−07 | 1.2E−06 | 2.1E−06 | 2.9E−06 | 4.0E−06 | 5.2E−06 |
| | | **1.17** | **1.16** | **1.10** | **0.98** | **0.98** | **1.03** | **1.34** | **1.30** | **1.23** | |
| | **BAY 1816032** | **BAY 1816032 plus AZ20** | | | | | | | | | **AZ20** |
| MDA-MB-468 | 3.7E−06 | 1.2E−06 | 8.9E−07 | 6.3E−07 | 5.3E−07 | 4.2E−07 | 3.1E−07 | 2.5E−07 | 2.0E−07 | 9.9E−08 | |
| | | 1.4E−07 | 2.2E−07 | 2.7E−07 | 3.6E−07 | 4.2E−07 | 4.6E−07 | 5.9E−07 | 8.2E−07 | 8.9E−07 | 1.3E−06 |
| | | **0.43** | **0.41** | **0.37** | **0.41** | **0.43** | **0.43** | **0.52** | **0.67** | **0.70** | |
| HT-144 | 3.0E−06 | 2.0E−06 | 9.1E−07 | 5.4E−07 | 3.7E−07 | 2.5E−07 | 1.7E−07 | 1.1E−07 | 6.4E−08 | 2.7E−08 | |
| | | 2.2E−07 | 2.3E−07 | 2.3E−07 | 2.5E−07 | 2.5E−07 | 2.5E−07 | 2.6E−07 | 2.6E−07 | 2.5E−07 | 2.4E−07 |
| | | **1.56** | **1.25** | **1.13** | **1.13** | **1.10** | **1.08** | **1.09** | **1.08** | **1.02** | |
| | **BAY 1816032** | **BAY 1816032 plus olaparib** | | | | | | | | | **Olaparib** |
| MDA-MB-436 | 2.3E−06 | 1.7E−06 | 1.5E−06 | 1.3E−06 | 1.0E−06 | 8.6E−07 | 7.2E−07 | 6.1E−07 | 5.3E−07 | 2.5E−07 | |
| | | 5.5E−07 | 1.2E−06 | 1.7E−06 | 2.0E−06 | 2.6E−06 | 3.2E−06 | 4.3E−06 | 6.4E−06 | 6.9E−06 | 1.1E−05 |
| | | **0.76** | **0.76** | **0.73** | **0.61** | **0.60** | **0.59** | **0.64** | **0.80** | **0.72** | |
| 22RV1 | 9.2E−07 | 6.8E−07 | 6.7E−07 | 6.1E−07 | 5.3E−07 | 5.1E−07 | 4.6E−07 | 3.8E−07 | 2.6E−07 | 1.7E−07 | |
| | | 2.3E−07 | 5.0E−07 | 7.9E−07 | 1.1E−06 | 1.5E−06 | 2.1E−06 | 2.7E−06 | 3.1E−06 | 4.6E−06 | 9.1E−06 |
| | | **0.77** | **0.78** | **0.76** | **0.70** | **0.72** | **0.72** | **0.70** | **0.62** | **0.69** | |

NOTE: $CI_{50}$ interpretation code: $CI_{50} < 0.8$, synergism; $0.8 \leq CI_{50} \leq 1.2$, additivity; $CI_{50} > 1.2$, antagonism. Calculated combination indices for 50% inhibition ($CI_{50}$) from proliferation assays of cell lines treated with drug combinations as indicated. Monotreatment $IC_{50}$ values and the concentrations required in combination of the two test compounds to achieve the $CI_{50}$ are shown. All concentrations are given in mol/L.

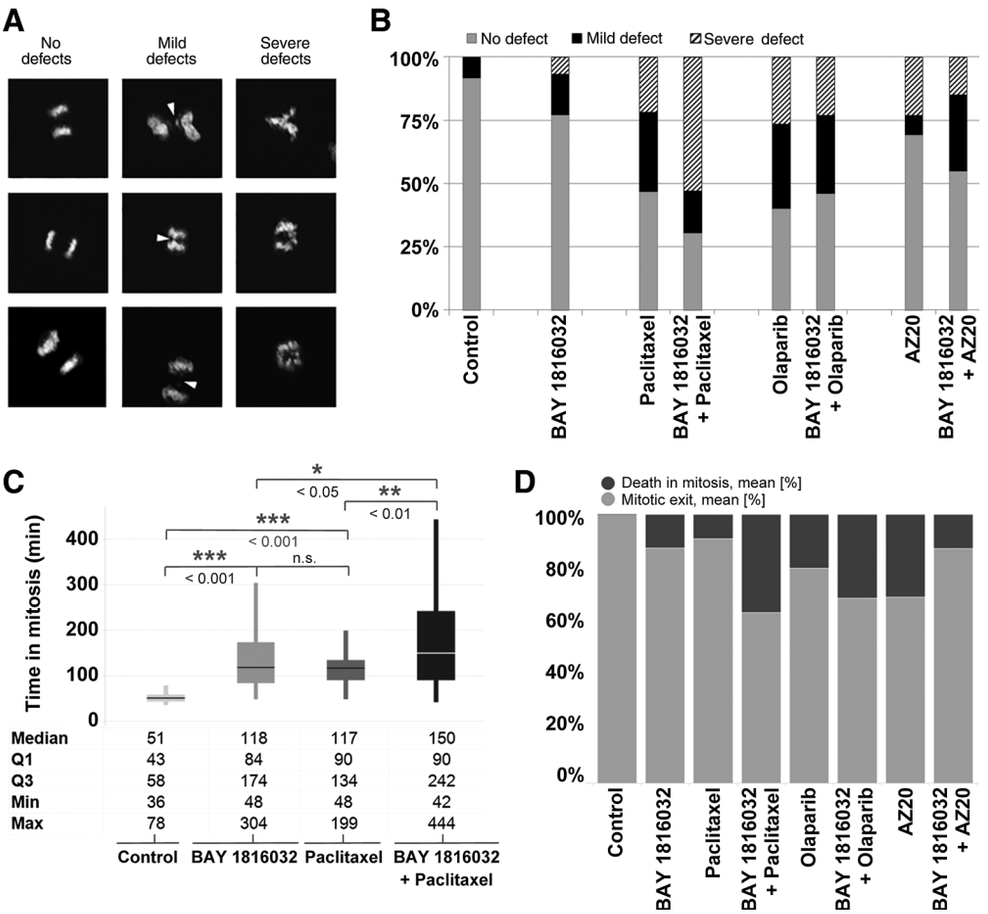


**Figure 2.**

BAY 1816032 treatment increases the rate of chromosomal segregation defects in combination with low doses of paclitaxel or ATR inhibitor. **A,** Time-lapse images of HeLa cells expressing H2B-GFP stably show chromosome separation defects that were used for cell fate classification in the experiments described under **B**; the arrowheads indicate chromosome bridges or delayed chromosomes: "no defect"; correct mitosis with bipolar separation of the sister chromatids, each daughter nucleus receives an identical half of the parental genome. "Mild defect"; during the condensation of the genome and the alignment of chromosomes toward the equatorial plate, delayed chromosomes can be recognized; time in mitosis is prolonged; the cell can successfully perform a bipolar separation of the genome. "Severe defects"; failure of correct arrangement of the chromosomes in the equatorial plate, a bipolar division of the genome cannot be recognized, observation of multinuclear daughter cells with inconsistent genome or cell death during or after mitosis. **B,** HeLa cells expressing H2B-GFP stably were treated with solvent (Control) or with paclitaxel (3 nmol/L), olaparib (5 μmol/L), or AZ20 (250 nmol/L) in the presence or absence of 1 μmol/L BAY 1816032 in triplicates and observed by fluorescence time-lapse imaging. The histograms show the frequency of chromosomal segregation defects according to the classification shown in **A** ($n = 100$ cells; all differences between the treatment groups were statistically significant. $P < 0.05$, unpaired $t$ test). **C,** Time in mitosis was determined for cells entering mitosis in the time frame of 10 to 24 hours after compound application. The period from the beginning of the prometaphase to the first image with an anaphase was determined (Mann–Whitney rank-sum test; n.s., not significant; *, $P < 0.05$; **, $P < 0.01$; ***, $P < 0.001$). **D,** Fate of cells entering mitosis 10 to 24 hours after compound application (BAY 1816032, and paclitaxel vs. control, $P < 0.005$; combination versus control, BAY 1816032, and paclitaxel, $P < 0.001$, Mann–Whitney rank-sum test).

ATM-proficient cells, as well as slight antagonism in ATM-deficient cells and upon combination with an ATM inhibitor indicating that the synergy between BUB1 and ATR inhibition requires the presence of active ATM (Supplementary Table S4). Previous publications indicated that ATM inhibition sensitizes cells against PARP inhibitors (31–33). On the basis of the hypothesis of BUB1 being a downstream target of ATM kinase, we investigated the effects of BAY 1816032 in combination with PARP inhibitors. In *BRCA1*-mutated MDA-MB-436 and in *BRCA2*-mutated 22RV1 cells, the combination with olaparib (Table 2) as well as with rucaparib and talazoparib (Supplementary Table S4) were synergistic, which may support the proposed role of BUB1 kinase downstream of ATM. To gain further insight into the mitotic effects of the BAY 1816032 combinations with paclitaxel, olaparib, and AZ20 on a cellular level, time series images of asynchronously growing HeLa cells expressing H2B-GFP were analyzed and the cell-cycle distribution of MDA-MB-436 and MDA-MB-468 cells was determined. Fluorescence time-lapse imaging was used to detect and quantify the frequencies of mild and severe chromosomal defects as classified according to the time-lapse stills shown in Fig. 2A. BUB1 kinase inhibition alone had only a minor effect on the frequency of chromosomal mis-segregation in HeLa cells. However, the combination with paclitaxel led to a strong increase in segregation defects, in particular in severe

defects (Fig. 2B). Median time in mitosis was extended by a factor of 2 upon single-agent BUB1 inhibitor and paclitaxel treatment, respectively, whereas the combination extended time in mitosis by a factor of 3 to 150 minutes (Fig. 2C). The increase in segregation defects was paralleled by an increase in the fraction of cells undergoing death in mitosis, in particular, upon combination of the BUB1 inhibitor with paclitaxel (Fig. 2D). A single treatment with olaparib increased the rate of chromosomal missegregation and death in mitosis in HeLa cells, while the combination with BUB1 inhibitor had no additional effect (Fig. 2B and D). Single-agent AZ20 ATR inhibitor treatment increased the rate of segregation defects, which was further increased upon combination with BAY 1816032, although mild defects were more prominent and the fraction of cells dying in mitosis was smaller in the combination group as compared with AZ20 single agent. Effects of treatment of MDA-MB-468 cells with BAY 1816032, AZ20, or the combination thereof on cell-cycle distribution were rather mild (Supplementary Fig. S3A). In the combination group, a slight increase in the number of cells with 4N DNA content was observed after 72 hours of treatment, which was statistically significant versus both single-agent groups ($P < 0.05$, $t$ test). Preliminary data ($n = 1$) indicated a slight increase of histone H3-Ser10 phosphorylation in the BAY 1816032 group, a slight decrease in the AZ20 group, and no change in the combination group as compared with vehicle control. Olaparib reduced the number of MDA-MB-436 cells with 2N DNA content ($P = 0.002$ vs. control, $P = 0.02$ vs. BAY 1816032 single agent, $t$ test), and increased the number of cells with 4N ($P = 0.01$ vs. control, $t$ test) and >4N DNA content after 72 hours of incubation (Supplementary Fig. S3B). In combination with BAY 1816032, these effects were slightly more pronounced and the increase in cells with >4N DNA content reached statistical significance versus the BAY 1816032 single-agent group ($P = 0.029$, $t$ test). These shifts in cell-cycle distribution, although rather mild upon combination of the compounds, are assumed to contribute to the observed more than additive effects on cell proliferation in the combination assays.

Our results of olaparib-induced segregation defects and accumulation of cells with 4N and >4N DNA content are in line with the finding that PARP trapping compromises replication fork stability and induces chromatin bridges, lagging chromosomes, and cytokinesis failure, in particular, in homologous recombination–deficient cells (34). Kabeche and colleagues (35) recently reported on a mitosis-specific and R loop–driven ATR pathway, which promotes faithful chromosome segregation. Inhibition of ATR kinase or depletion of ATR reduced phosphorylation and activity of AURKB kinase and increased the rate of lagging chromosomes but did not affect the centromeric localization of AURKB and other components of the chromosome passenger complex indicating that ATR is required for full activation of AURKB and microtubule attachment error correction. BUB1 kinase inhibition led to a partial dyslocalization of chromosome passenger complex components including AURKB and a partial reduction of AURKB activity at centromeres (10). The combined ATR and BUB1 kinase inhibition may further compromise AURKB-mediated error correction and cause the observed more than additive antiproliferative activity upon combination treatment. After submission of the manuscript, Li and colleagues (36) reported on the requirement of BUB1 kinase activity to resolve replication stress induced by telomeric G-quadruplexes and to facilitate telomere replication. Whether these newly discovered functions of ATR and BUB1 are the basis for the synergistic interaction with ATR inhibition will be the topic of future investigations.

Having shown that BAY 1816032 is a highly selective BUB1 kinase inhibitor that specifically inhibits BUB1 intracellular signaling and interacts with clinically relevant concentrations of paclitaxel and docetaxel, as well as with PARP and ATR inhibitors in a synergistic manner, we next investigated its pharmacokinetic and toxicologic properties.

### Pharmacokinetic and toxicologic characterization

Pharmacokinetic parameters were determined in mouse, rat, and dog. Following intravenous administration of BAY 1816032 as bolus of 1.0 mg/kg to male CD1 mouse and to male Wistar rat, as well as 15-minute infusion of 0.5 mg/kg to female Beagle dog, the compound exhibited different blood clearances across the species, moderate in mouse and rat, and low in dog. The volumes of distribution at steady state (Vss) were high and terminal half-lives were intermediate in mouse and long in rat and dog. After oral administration of 1 mg/kg to female NMRI mouse, 5 mg/kg to male Wistar rat, and 0.5 mg/kg to Beagle dog, a fast absorption was observed. The oral bioavailability was low in mouse and moderate in rat and dog (Table 3).

Exploratory two-week repeat-dose toxicity studies were performed in Wistar rat and Beagle dog. BAY 1816032 was administered orally once daily to groups of 6 male rats at doses of 25, 50, or 100 mg/kg/day, whereas one male and one female dog per group were dosed at 10 and 40 mg/kg/day. In-life parameters included clinical observations, body weight, food and water consumption, ECG and blood pressure (dog only), blood clinical chemistry, and hematology. At necropsy, gross pathology was performed. Organ weights were determined and histology was performed with a focus on key organs and tissues expected to be target due to the mode of action. No treatment-related effects were detected in the abovementioned endpoints for both species. The exposures were up to 20-fold in rat and up to 7-fold in dog above the efficacious exposure in mice. The observed safety profile is in line with data from knockin mice with an inactive BUB1 kinase which had the same phenotype as wild-type mice (9).

**Table 3.** Mean pharmacokinetic parameters of BAY 1816032 after single administration in preclinical species

| | Intravenous administration | | | | | Intragastric (p.o.) administration | | | | | |
|---|---|---|---|---|---|---|---|---|---|---|---|
| **Species** | **Sex** | **Dose (mg/kg)** | **$T_{1/2}$ (h)** | **$V_{ss}$ (L/kg)** | **$CL_{blood}$ (L/h/kg)** | **Sex** | **Dose (mg/kg)** | **$T_{max}$ (h)** | **$T_{1/2}$(h)** | **$C_{max,\ norm}$ (μg/L)** | **F (%)** |
| Mouse | F | 1.0 | 1.8 | 4.0 | 3.7 | F | 1.0 | 0.25 | 1.8 | 0.024 | 22 |
| Rat | M | 1.0 | 3.9 | 4.5 | 1.7 | M | 5.0 | 7.0 | 5.8 | 0.054 | 60 |
| Dog | F | 0.5 | 4.2 | 2.5 | 0.56 | F | 0.5 | 1.0 | 4.7 | 0.17 | 59 |

NOTE: routes of administration: mouse and rat, intravenous administration as bolus; dog, infusion (15 minutes).

Abbreviations: $C_{max,\ norm}$, dose-normalized maximum plasma concentration; $CL_{blood}$, blood clearance; F, bioavailability; F, female; M, male $T_{1/2}$, half-life; $T_{max}$, time point of maximum plasma concentration; $V_{SS}$, volume of distribution at steady state.

Taken together these data indicate that BAY 1816032 exhibits a favorable pharmacokinetic profile and high safety margins, supporting further development for clinical application.

**Cooperative activity of BAY 1816032 with paclitaxel or olaparib in tumor xenograft models**

Having confirmed oral bioavailability and systemic exposure, we intended to transfer the *in vitro* combination results with taxanes and PARP inhibitors to tumor xenograft models. To this end, we evaluated the combination of BAY 1816032 with paclitaxel and with olaparib in models of triple-negative breast cancer. For the paclitaxel combination, we selected the SUM-149 model that shows an adaptive resistance toward paclitaxel and tumor outgrowth under treatment after initial response. Treatment of tumor-bearing female nude mice with BAY 1816032 as single agent did not show any significant effect on the growth of SUM-149 tumors (Fig. 3A). Paclitaxel initially suppressed tumor growth; however, starting around day 28, tumors gained size and grew out although the dose of paclitaxel had been increased from 8 mg/kg to the MTD of 20 mg/kg from day 24 onward. In contrast, the tumors from the BAY 1816032 plus paclitaxel combination treatment group grew much slower and entered a phase of stable disease around day 46. An analysis of the median tumor areas of the paclitaxel single-agent group and the combination group at day 54 showed a statistically significant difference between the two treatment groups ($P < 0.05$, ANOVA on ranks). The treatments were well tolerated with no treatment-related animal deaths and maximal body weight loss of 2% in the vehicle control group and 2.4 % in the BAY 1816032 plus paclitaxel combination group.

Plasma levels and AUCs of paclitaxel and BAY 1816032 upon the last single agent and combination treatments were determined. The AUC of paclitaxel in the BAY 1816032 combination group was slightly below the AUC in the single-agent group, similarly the AUC of BAY 1816032 in combination with paclitaxel was found slightly below the AUC of BAY 1816032 as single agent, indicating that increased combination efficacy was not driven by pharmacokinetic drug–drug interactions (Supplementary Table S5). Evaluation of histologic skin samples stained for Thr120-phosphorylated histone H2A upon treatment of mice either with single-agent paclitaxel or with combinations of paclitaxel with various doses of BAY 1816032 demonstrated a dose-dependent reduction in the number of H2A phospho-Thr120–positive cells indicative of BUB1 kinase inhibition by BAY 1816032 *in vivo* (Fig. 3B).

The *in vivo* activity of the combination of the BUB1 kinase inhibitor with the PARP inhibitor olaparib was evaluated in the *BRCA1*-mutated MDA-MB-436 triple-negative breast cancer model (Fig. 3C). On day 69 (42 days after start of treatment), when the vehicle control group had to be terminated for animal welfare reasons (violation of limit in tumor size), BAY 1816032 single-agent treatment showed almost no efficacy (T/C 0.82), whereas olaparib was moderately active (T/C 0.47), and the BAY 1816032 plus olaparib combination showed a strong tumor growth inhibition (T/C 0.22). Tumor growth of the combination group was much slower as compared with the olaparib single-agent treatment group until the end of the study on day 91 (64 days after start of treatment). Finally, the mean tumor area of the combination group was 65% below the olaparib single-agent group and the difference was statistically significant ($P < 0.001$, one-way ANOVA, *t* test). The data from the orthotopically grown triple-negative human breast cancer model clearly demonstrated the more than additive antitumor efficacy of the combination of BAY 1816032 with a PARP inhibitor, in particular, with respect to the outgrowth of the tumors under continued treatment.

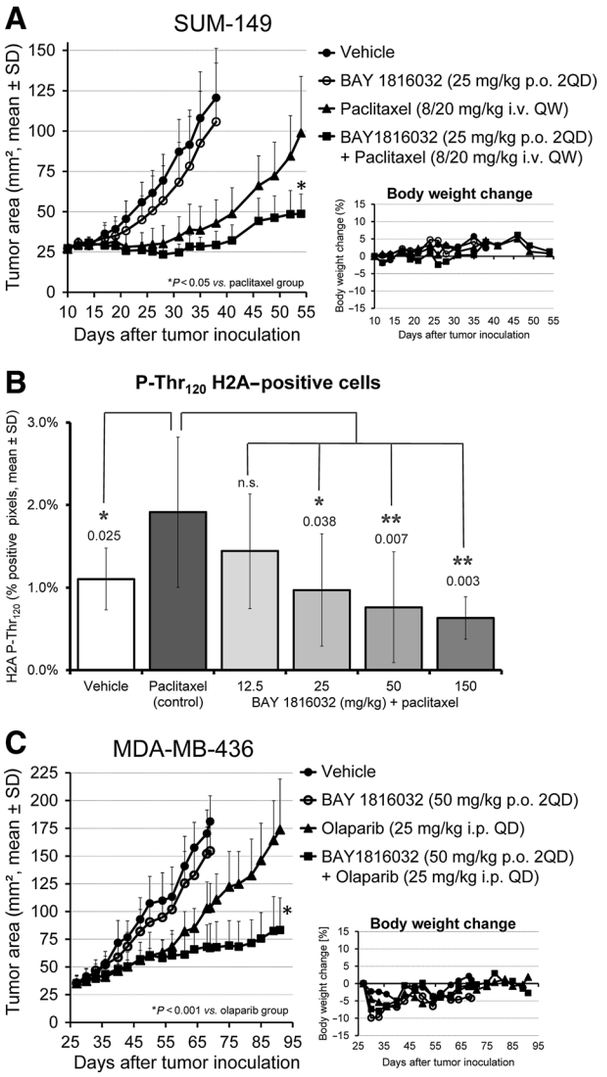


**Figure 3.**

Response of human xenograft tumors to BAY 1816032 in combination with paclitaxel or olaparib. **A,** SUM-149 human triple-negative breast cancer cells were implanted subcutaneously into nude mice on day 0 (12 animals/group). Treatment was started on day 10 when tumors had reached a size of approximately 27 mm$^2$. **B,** Nude mice (3 animals/ group) were treated with paclitaxel (once, 20 mg/kg) and BAY 1816032 (3 times). Skin samples were taken 4 hours after the last treatment and stained for phospho-Thr120 histone H2A. *P* values were determined by means of unpaired *t* test analysis. **C,** MDA-MB-436 human triple-negative breast cancer cells were implanted orthotopically into the fad pad in NOD-SCID mice (12 animals/group). Treatment was started on day 27 when tumors had reached a size of approximately 35 mm$^2$. BAY 1816032 was administered orally (p.o.) twice daily (2QD); paclitaxel was administered intravenously (i.v.) once per week (QW); olaparib was administered intraperitoneal (i.p.) once daily (QD). Tumor growth was monitored by determination of the tumor area using caliper measurement three times weekly. n.s., not significant; *, $P < 0.05$; **, $P < 0.01$.

## Discussion

Recent findings suggested that BUB1 kinase activity is required for chromosome arm resolution and positioning of the chromosomal passenger complex for resolution of spindle attachment errors and plays only a minor role in spindle assembly checkpoint activation. Because of their tubulin-stabilizing mode of action taxanes increase the rate of attachment errors, which led to our hypothesis that inhibition of the spindle attachment error correction mechanisms could improve the efficacy of taxanes. Taxanes still represent the standard-of-care for cancer treatment in many tumor indications. Recently, PARP inhibitors were introduced as treatment option for *BRCA1/2*–mutated ovarian cancers and are currently being evaluated in combination treatments with DNA-damaging agents and DNA damage response inhibitors. However, development of resistance mechanisms leading to tumor recurrence highlight the medical need for improved treatment options. Using the novel BUB1 kinase inhibitor BAY 1816032, we showed *in vitro* additive and more than additive (synergistic) activity in combination with paclitaxel and docetaxel, as well as with ATR and PARP inhibitors targeting DNA damage response and repair. Because of the favorable pharmacokinetic profile and good tolerability of BAY 1816032, we were able to transfer the *in vitro* combination results to relevant *in vivo* tumor models. BUB1 kinase inhibition in combination with paclitaxel or PARP inhibitor treatment resulted in significant reduction and delay of tumor outgrowth under treatment as compared with the single agents. Previously, inhibitors of other SAC kinases were identified and underwent preclinical and clinical investigations. AURKB inhibitors showed myelosuppression, in particular neutropenia, as dose-limiting toxicities in clinical trials (reviewed in ref. 37) and MPS1 inhibitors were reported to induce severe gastrointestinal toxicities and neutropenia in preclinical species (14, 38). The remarkably clean toxicologic profile of BAY 1816032 and the good tolerability in xenograft studies clearly distinguishes the BUB1 kinase inhibitor from compounds targeted against Aurora and MPS1 kinases. These findings suggest clinical proof-of-concept studies evaluating the BUB1 kinase inhibitor BAY 1816032 in combination with taxanes or PARP inhibitors to enhance their efficacy and potentially suppress or delay the development of therapy resistance.

## Disclosure of Potential Conflicts of Interest

F. von Nussbaum has ownership interests (including patents) in Bayer and is a consultant/advisory board member for German Chemical Society and EFMC-ISMC. M. Brands and K. Ziegelbauer have ownership interests (including patents) in Bayer. No potential conflicts of interest were disclosed by the other authors.

## Authors' Contributions

**Conception and design:** G. Siemeister, A.E. Fernández-Montalván, W. Bone, S. Zitzmann-Kolbe, S. Prechtl, M. Hitchcock, F. von Nussbaum, K. Ziegelbauer
**Development of methodology:** G. Siemeister, A.E. Fernández-Montalván, J. Schröder, S. Prechtl, S.J. Holton, O. von Ahsen, V. Pütter, M. Hitchcock, F. von Nussbaum
**Acquisition of data (provided animals, acquired and managed patients, provided facilities, etc.):** G. Siemeister, A.E. Fernández-Montalván, W. Bone, S. Zitzmann-Kolbe, S. Prechtl, S.J. Holton, M. Hitchcock
**Analysis and interpretation of data (e.g., statistical analysis, biostatistics, computational analysis):** G. Siemeister, A.E. Fernández-Montalván, W. Bone, J. Schröder, S. Zitzmann-Kolbe, H. Briem, S. Prechtl, S.J. Holton, U. Mönning, O. von Ahsen, S. Johanssen, M. Hitchcock, F. von Nussbaum
**Writing, review, and/or revision of the manuscript:** G. Siemeister, A.E. Fernández-Montalván, W. Bone, H. Briem, O. von Ahsen, F. von Nussbaum, D. Mumberg
**Study supervision:** G. Siemeister, W. Bone, S. Zitzmann-Kolbe, U. Mönning, S. Johanssen, M. Brands, K. Ziegelbauer, D. Mumberg
**Others (designed compounds and developed strategies for optimization):** A. Mengel
**Others (ran xenograft studies):** W. Bone
**Others (ran *in vitro* cellular studies, designed, and supervised studies and interpreted results):** S. Prechtl
**Others (design and performance of pharmacokinetic studies to assess ADME properties):** U. Mönning
**Others (designed compounds and developed strategies for optimization):** A. Cleve

## Acknowledgments

We thank Dennis Brinckmann, Nicole Dittmar, Ivonne Herms, Katja Kauffeldt, Robert Karmauss, Martin Kohs, Sylwia Kubicka, Thomas Kuhles, Anne Mattstedt, Sebastian Räse, Elke Schmid, Volker Stickel, Carmen Wegner, Franziska Woisch, Henk Zimmermann for excellent technical assistance, and Jörg Fanghänel and Christian Stegmann for ITC measurements.

The costs of publication of this article were defrayed in part by the payment of page charges. This article must therefore be hereby marked *advertisement* in accordance with 18 U.S.C. Section 1734 solely to indicate this fact.

Received February 23, 2018; revised July 3, 2018; accepted November 8, 2018; published first November 14, 2018.

## References

1. Hanahan D, Weinberg RA. The hallmarks of cancer. Cell 2000;100:57–70.
2. Dominguez-Brauer C, Thu KL, Mason JM, Blaser H, Bray MR, Mak TW. Targeting mitosis in cancer: emerging strategies. Mol Cell 2015;60:524–36.
3. Musacchio A. The molecular biology of spindle assembly checkpoint signaling dynamics. Curr Biol 2015;25:R1002–18.
4. Primorac I, Weir JR, Chiroli E, Gross F, Hoffmann I, van Gerwen S, et al. Bub3 reads phosphorylated MELT repeats to promote spindle assembly checkpoint signaling. Elife 2013;2:e01030.
5. Overlack K, Primorac I, Vleugel M, Krenn V, Maffini S, Hoffmann I, et al. A molecular basis for the differential roles of Bub1 and BubR1 in the spindle assembly checkpoint. Elife 2015;4:e05269.
6. Faesen AC, Thanasoula M, Maffini S, Breit C, Muller F, van Gerwen S, et al. Basis of catalytic assembly of the mitotic checkpoint complex. Nature 2017;542:498–502.
7. Kawashima SA, Yamagishi Y, Honda T, Ishiguro K, Watanabe Y. Phosphorylation of H2A by Bub1 prevents chromosomal instability through localizing shugoshin. Science 2010;327:172–7.
8. Wang F, Ulyanova NP, van der Waal MS, Patnaik D, Lens SM, Higgins JM. A positive feedback loop involving Haspin and Aurora B promotes CPC accumulation at centromeres in mitosis. Curr Biol 2011;21:1061–9.
9. Ricke RM, Jeganathan KB, Malureanu L, Harrison AM, van Deursen JM. Bub1 kinase activity drives error correction and mitotic checkpoint control but not tumor suppression. J Cell Biol 2012;199:931–49.
10. Baron AP, von Schubert C, Cubizolles F, Siemeister G, Hitchcock M, Mengel A, et al. Probing the catalytic functions of Bub1 kinase using the small molecule inhibitors BAY-320 and BAY-524. Elife 2016;17:12187.
11. Krenn V, Musacchio A. The aurora B kinase in chromosome bi-orientation and spindle checkpoint signaling. Front Oncol 2015;5:225.
12. Hitchcock M, Mengel A, Pütter V, Siemeister G, Wengner AM, Briem H, et al. inventors; Bayer Pharma AG, Bayer Intellectual Property GmbH, assignee. Substituted benzylindazoles for use as BUB1 kinase inhibitors in the treatment of hyperproliferative diseases. Patent WO2013050438. 2013 Apr 11.

13. Copeland RA. Evaluation of enzyme inhibitors in drug discovery: a guide for medicinal chemists and pharmacologists Methods Biochem Anal 2005;46:1–265.
14. Martinez R, Blasina A, Hallin JF, Hu W, Rymer I, Fan J, et al. Mitotic checkpoint kinase Mps1 has a role in normal physiology which impacts clinical utility. PLoS One 2015;10:e0138616.
15. Collaborative Computational Project. The CCP4 suite: programs for protein crystallography. Acta Crystallogr D Biol Crystallogr 1994;50:760–3.
16. Kabsch W. XDS. Acta Crystallogr D Biol Crystallogr 2010;66:125–32.
17. McCoy AJ, Grosse-Kunstleve RW, Adams PD, Winn MD, Storoni LC, Read RJ. Phaser crystallographic software. J Appl Crystallogr 2007;40:658–74.
18. Emsley P, Lohkamp B, Scott WG, Cowtan K. Features and development of Coot. Acta Crystallogr D Biol Crystallogr 2010;66:486–501.
19. Wengner AM, Siemeister G, Koppitz M, Schulze V, Kosemund D, Klar U, et al. Novel Mps1 kinase inhibitors with potent antitumor activity. Mol Cancer Ther 2016;15:583–92.
20. Mengel A, Lerchen HG, Möwes M, Müller T, Bärfacker L, Hitchcock M, et al. inventors; Bayer Pharma AG, assignee. Benzyl substituted indazoles as bub1 inhibitors. Patent WO2016042084. 2016 Mar 24.
21. Viswanatha R, Ohouo PY, Smolka MB, Bretscher A. Local phosphocycling mediated by LOK/SLK restricts ezrin function to the apical aspect of epithelial cells. J Cell Biol 2012;199:969–84.
22. Kang J, Yang M, Li B, Qi W, Zhang C, Shokat KM, et al. Structure and substrate recruitment of the human spindle checkpoint kinase Bub1. Mol Cell 2008;32:394–405.
23. Nyati S, Schinske-Sebolt K, Pitchiaya S, Chekhovskiy K, Chator A, Chaudhry N, et al. The kinase activity of the Ser/Thr kinase BUB1 promotes TGF-beta signaling. Sci Signal 2015;8:ra1.
24. Inman GJ, Nicolas FJ, Callahan JF, Harling JD, Gaster LM, Reith AD, et al. SB-431542 is a potent and specific inhibitor of transforming growth factor-beta superfamily type I activin receptor-like kinase (ALK) receptors ALK4, ALK5, and ALK7. Mol Pharmacol 2002;62:65–74.
25. Yang C, Wang H, Xu Y, Brinkman KL, Ishiyama H, Wong ST, et al. The kinetochore protein Bub1 participates in the DNA damage response. DNA Repair 2012;11:185–91.
26. Reaper PM, Griffiths MR, Long JM, Charrier JD, Maccormick S, Charlton PA, et al. Selective killing of ATM- or p53-deficient cancer cells through inhibition of ATR. Nat Chem Biol 2011;7:428–30.
27. Foote KM, Blades K, Cronin A, Fillery S, Guichard SS, Hassall L, et al. Discovery of 4-{4-[(3R)-3-Methylmorpholin-4-yl]-6-[1-(methylsulfonyl) cyclopropyl]pyrimidin-2-y l}-1H-indole (AZ20): a potent and selective inhibitor of ATR protein kinase with monotherapy *in vivo* antitumor activity. J Med Chem 2013;56:2125–38.
28. Vendetti FP, Lau A, Schamus S, Conrads TP, O'Connor MJ, Bakkenist CJ. The orally active and bioavailable ATR kinase inhibitor AZD6738 potentiates the anti-tumor effects of cisplatin to resolve ATM-deficient non-small cell lung cancer *in vivo*. Oncotarget 2015;6:44289–305.
29. Hall AB, Newsome D, Wang Y, Boucher DM, Eustace B, Gu Y, et al. Potentiation of tumor responses to DNA damaging therapy by the selective ATR inhibitor VX-970. Oncotarget 2014;5:5674–85.
30. Luecking UT, Lefranc J, Wengner AM, Wortmann L, Schick H, Briem H, et al. Identification of potent, highly selective and orally available ATR inhibitor BAY 1895344 with favorable PK properties and promising efficacy in monotherapy and combination in preclinical tumor models [abstract]. In Proceedings of the AACR 2017 Annual Meeting; 2017 Apr 1–5; Washington, DC. Philadelphia (PA): AACR; 2017. Abstract nr 983.
31. McCabe N, Turner NC, Lord CJ, Kluzek K, Bialkowska A, Swift S, et al. Deficiency in the repair of DNA damage by homologous recombination and sensitivity to poly(ADP-ribose) polymerase inhibition. Cancer Res 2006;66:8109–15.
32. Kubota E, Williamson CT, Ye R, Elegbede A, Peterson L, Lees-Miller SP, et al. Low ATM protein expression and depletion of p53 correlates with olaparib sensitivity in gastric cancer cell lines. Cell Cycle 2014;13:2129–37.
33. Williamson CT, Muzik H, Turhan AG, Zamo A, O'Connor MJ, Bebb DG, et al. ATM deficiency sensitizes mantle cell lymphoma cells to poly(ADP-ribose) polymerase-1 inhibitors. Mol Cancer Ther 2010;9:347–57.
34. Schoonen PM, Talens F, Stok C, Gogola E, Heijink AM, Bouwman P, et al. Progression through mitosis promotes PARP inhibitor-induced cytotoxicity in homologous recombination-deficient cancer cells. Nat Commun 2017;8:15981.
35. Kabeche L, Nguyen HD, Buisson R, Zou L. A mitosis-specific and R loop-driven ATR pathway promotes faithful chromosome segregation. Science 2018;359:108–14.
36. Li F, Kim H, Ji Z, Zhang T, Chen B, Ge Y, et al. The BUB3-BUB1 complex promotes telomere DNA replication. Mol Cell 2018;70:395–407.e4.
37. Falchook GS, Bastida CC, Kurzrock R. Aurora kinase inhibitors in oncology clinical trials: current state of the progress. Semin Oncol 2015;42:832–48.
38. Maia AR, de Man J, Boon U, Janssen A, Song JY, Omerzu M, et al. Inhibition of the spindle assembly checkpoint kinase TTK enhances the efficacy of docetaxel in a triple-negative breast cancer model. Ann Oncol 2015; 26:2180–92.
39. Cheng Y, Prusoff WH. Relationship between the inhibition constant (K1) and the concentration of inhibitor which causes 50 per cent inhibition (I50) of an enzymatic reaction. Biochem Pharmacol 1973;22:3099–108.
40. Motulsky HJ, Mahan LC. The kinetics of competitive radioligand binding predicted by the law of mass action. Mol Pharmacol 1984;25:1–9.